J. Fluid Mech. (1968), *vol.* 32, *part* 2, *pp.* 251–272
Printed in Great Britain

On slow transverse flow past obstacles in a rapidly rotating fluid†

By R. HIDE‡

Department of Geology and Geophysics and Department of Physics
Massachusetts Institute of Technology, Cambridge, Massachusetts 02139, U.S.A.

AND A. IBBETSON§

Woods Hole Oceanographic Institution, Woods Hole, Massachusetts 02543, U.S.A.

Appendix

By M. J. LIGHTHILL

Imperial College, London

(Received 5 April 1967 and in revised form 10 October 1967)

This paper describes an experimental and theoretical study of the complicated disturbance (Taylor column) due to the slow relative motion between a spherical, or short cylindrical, rigid object and an incompressible fluid of low viscosity in which the object is immersed, when the motion of the object is that of steady revolution with angular speed Ω rad/sec about an axis (the Z-axis) whose perpendicular distance from the centre of the object, $\bar{R}$, is much greater than a typical linear dimension of the object, L, and the undisturbed fluid motion is one of steady rotation about the same axis with angular speed $(\Omega + U_\vartheta/R)$ and zero relative vorticity (i.e. $d(U_\vartheta R)/dR = 0$). It extends earlier experimental work on Taylor columns to systems of sufficiently large axial dimensions for Z variations in the disturbance pattern to be perceptible. Over the ranges of Rossby and Ekman numbers (based on L) covered by the experiments, namely $\epsilon = 1{\cdot}89 \times 10^{-3}$ to $2{\cdot}36 \times 10^{-1}$ and $\gamma = 1{\cdot}30 \times 10^{-3}$ to $2{\cdot}03 \times 10^{-2}$ respectively, the axis of the Taylor column is found to trail in the downstream direction at a small angle $\psi = \tan^{-1}(K\epsilon)$ to the line parallel to the Z-axis through the centre of the object, where $K = (1{\cdot}54 \pm 0{\cdot}04)$ for a sphere. The variation with Z of the amplitude of the disturbance is roughly linear and the scale-length of this variation, Z_c, is close to $L/\gamma^{\frac{1}{4}}$ over the limited range of γ covered by the experiments.

The experimental value of K is remarkably close to the theoretical value derived by Prof. Lighthill in the appendix, where he applies his general linear theory of waves generated in a dispersive system by travelling forcing effects to the problem of describing a Taylor column at large distances from the moving object when the fluid is inviscid and unbounded.

---

† Contribution No. 1932 from the Woods Hole Oceanographic Institution.
‡ Now at the Meteorological Office, Bracknell, Berkshire, England.
§ Now at the School of Physics, University of Newcastle upon Tyne.

1. Introduction

Consider an annular cavity bounded by rigid, concentric, cylindrical side-walls in $R = R_i$ and $R = R_o$ and by rigid, plane, parallel end-walls in $Z = \frac{1}{2}D$ and $Z = -\frac{1}{2}D$ (the cylindrical polar co-ordinates of a general point referred to the axis of the side-walls being (R, ϑ, Z)). Suppose the cavity to be filled completely with an incompressible homogeneous fluid in steady motion, Eulerian flow velocity $\mathbf{u} = \mathbf{U}$, relative to the walls of the cavity where, except within boundary layers on the cavity walls, $\mathbf{U} = (0, U_\vartheta, 0)$, where RU_ϑ is a constant, so that $\nabla \times \mathbf{U} = 0$.

The present paper is concerned with the effects of rapid uniform rotation of the whole system with angular velocity $\mathbf{\Omega} = (0, 0, \Omega)$ on the disturbance caused by the presence in the fluid of a small, rigid object of axial dimensions equal to h and transverse dimensions equal to L, fixed in position relative to the walls of the cavity with its centre at $(\bar{R}, \bar{\vartheta}, \bar{Z})$, where $\bar{R} \sim \frac{1}{2}(R_o + R_i)$, $\bar{Z} = 0$, and h and L are both much less than D and $(R_o - R_i)$. It thus extends earlier work on 'Taylor columns' (to which slow flows past obstacles generally give rise in rapidly rotating fluids) to a system with sufficiently large axial dimensions for Z variations in the disturbance pattern, as well as other details of the flow, to be perceptible.

The rotation rate is considered rapid and the relative motion slow when the Ekman and Rossby numbers, in this case defined as follows (cf. equations (2.6))

$$\gamma \equiv 2\nu/L^2\Omega, \quad \epsilon = |U_\vartheta(\bar{R})|/\Omega L \tag{1.1a,b}$$

(where ν is the coefficient of kinematical viscosity) are both much less than unity, regarding $\frac{1}{2}L$ as a typical transverse dimension of the system and $U_\vartheta(\bar{R})$ as a typical relative flow velocity, V, (see equations (2.6)). Generally, in the hypothetical limit when $\epsilon \to 0$ and $\gamma \to 0$,

$$\partial \mathbf{u}/\partial Z = 0 \tag{1.2}$$

everywhere (see Proudman 1916, also equation (2.5) below), except in certain singular regions, where discontinuities may arise. Taylor (1923) recognized that equation (1.2) is only satisfied by the field of hydrodynamical flow due to the slow motion of a three-dimensional object through a rapidly rotating fluid when the column of fluid that stretches out parallel to the Z axis from all points on the surface of the object to the axial extremities of the fluid is carried along with the object, and demonstrated the tendency for such a column to form by towing a short cylinder through a rotating tank of fluid.

The walls of the hypothetical 'Taylor column' that occurs when $\gamma = \epsilon = 0$ are singular regions, where the tangential component of $\mathbf{u}$ may be discontinuous. In practice, of course, neither γ nor ϵ can equal zero, but when $(\gamma + \epsilon) \ll 1$ equation (1.2) is satisfied nearly everywhere to zeroth order in $(\gamma + \epsilon)$ (see equation (2.5*b*)). Most of the flow is then quasi-geostrophic, the force balance being between Coriolis and pressure forces, to zeroth order in $(\gamma + \epsilon)$ (see equation (2.5*a*)). $\mathbf{u}$ is not, however, completely determined by (1.2), and it is necessary therefore to

remove the associated degeneracy by considering ageostrophic effects also. Such effects become pronounced and even dominant in the vicinity of the walls of the hypothetical Taylor column and in boundary layers that occur on the bounding surfaces of the system.

All theoretical investigations relating to Taylor columns have been such that either $\gamma = 0$ or $\epsilon = 0$, inertial forces being responsible for ageostrophic effects in the former case, viscous forces in the latter (see § 2). Unfortunately, it is hard in practice to achieve the conditions (namely $\epsilon \ll \gamma^{\frac{1}{2}}$) under which the strictly viscous case, $\gamma \neq 0$, $\epsilon = 0$, applies (see § 2). On the other hand, conditions under which viscous effects are altogether negligible are also hard to achieve, so that any completely realistic comparison of theory with experiment has to contend with both viscous and inertial effects.

Denote by Z_c the length-scale characteristic of the Z variation of the amplitude of the disturbance, and by ψ the angle between the 'axis' of the disturbed region and the line $R = \bar{R}$, $\vartheta = \bar{\vartheta}$. Z_c and ψ depend on ϵ and γ; by equation (1.2) $\psi = 0$ and $Z_c = \infty$ when $\epsilon = \gamma = 0$. The present investigation stems from an unpublished study of Taylor columns by one of us (R. H.) and Mr T. Greenfield, who observed, more or less incidentally when using an apparatus for which ϵD was somewhat greater than in previous experiments, that the axis of the Taylor columns trailed downstream of the obstacle at a small angle, ψ, of the order of ϵ.

In what follows an outline of previous work is given first (see § 2). Then, in § 3, an account is presented of the apparatus used in the present work, including the theory of its operation, and various experimental techniques. Section 4 describes experiments on flow past a sphere, diameter $2a = L(=h) = 2{\cdot}54$ cm. Measurements of ψ made at 9 values of ϵ ranging from 0·0138 to 0·236 (γ being kept constant at $1{\cdot}36 \times 10^{-3}$), yield the expression

$$\tan\psi = K\epsilon, \tag{1.3a}$$

where

$$K = (1{\cdot}54 \pm 0{\cdot}04) \quad \text{(standard errors)} \tag{1.3b}$$

for the empirical relationship between ψ and ϵ. Section 5 describes a brief study of flow past a cylinder, and § 6 an investigation of viscous effects on flow past a sphere, in which an attempt was made to achieve conditions under which viscous effects dominate inertial effects. Such conditions probably were achieved at the highest values of γ and the lowest values of ϵ attained, namely $2{\cdot}03 \times 10^{-2}$ and $1{\cdot}89 \times 10^{-3}$ respectively. The few determinations that were made of Z_c, the axial extent of the disturbed region, suggest tentatively that $Z_c \sim L\gamma^{-\frac{1}{4}}$.

Finally, in the appendix, Prof. Lighthill applies his general linear theory of waves generated in a dispersive system by travelling forcing effects (Lighthill 1967) to the problem of describing the structure of a Taylor column at large distances from a moving object in an inviscid, unbounded fluid. It is remarkable how well linear theory can account for certain characteristics of the disturbance, including the value of K, near the obstacle.

2. Basic equations and outline of previous work

The equations of motion governing the flow of an incompressible fluid of uniform density relative to a frame of reference rotating with angular velocity $\boldsymbol{\Omega} = (0, 0, \Omega)$ are

$$\frac{\partial \mathbf{u}}{\partial t} + (\mathbf{u}.\nabla)\,\mathbf{u} + 2\boldsymbol{\Omega} \times \mathbf{u} = -\nabla P + \nu \nabla^2 \mathbf{u} \tag{2.1}$$

and

$$\nabla . \mathbf{u} = 0, \tag{2.2}$$

where P is the dynamic pressure (i.e. total pressure minus the pressure associated with gravitational and centrifugal forces) divided by density. Eliminate P and thus find for the relative vorticity,

$$\boldsymbol{\omega} \equiv \nabla \times \mathbf{u}, \tag{2.3}$$

the equation

$$\frac{\partial \boldsymbol{\omega}}{\partial t} + [(\mathbf{u}.\nabla)\,\boldsymbol{\omega} - (\boldsymbol{\omega}.\nabla)\,\mathbf{u}] - \nu \nabla^2 \boldsymbol{\omega} = 2\Omega \frac{\partial \mathbf{u}}{\partial Z}. \tag{2.4}$$

According to (2.1) and (2.4), when $\gamma \ll 1$ and $\epsilon \ll 1$

$$|\nabla P| + |2\boldsymbol{\Omega} \times \mathbf{u}| \sim \Omega V(\epsilon + \gamma) \tag{2.5a}$$

and

$$\left|\frac{\partial \mathbf{u}}{\partial Z}\right| \sim \frac{V}{L}(\gamma + \epsilon), \tag{2.5b}$$

V being a typical relative flow speed, where, in general,

$$\gamma \equiv 2\nu/\Omega L^2, \quad \epsilon \equiv (2\Omega\tau)^{-1} + V/L\Omega \tag{2.6a, b}$$

(cf. equations (1.1)), τ being a time-scale characteristic of non-steady features of the flow pattern. It is in the limit $\gamma = \epsilon = 0$ that geostrophic balance and the Proudman–Taylor theorem (cf. equation (1.2)), as expressed by the equations

$$\nabla P + 2\boldsymbol{\Omega} \times \mathbf{u} = 0, \quad \partial \mathbf{u}/\partial Z = 0, \tag{2.7a, b}$$

hold exactly. As already noted in § 1, although equations (2.7) are closely satisfied when $\gamma \ll 1$ and $\epsilon \ll 1$, the essential degeneracy present in these equations can only be resolved by considering also those limited regions of the fluid where pronounced ageostrophic effects occur.

It will be convenient to make use of expressions for the balance of ζ, the Z component of $\boldsymbol{\omega}$, and of $\bar{\zeta}$, the mean (with respect to Z) value of ζ for an axial fluid filament whose ends terminate at the axial extremities of the fluid, in $Z = Z_l$ and $Z = Z_u$, $(Z_l < Z_u)$.

Consider the Z component of (2.4) when, owing to the slow average rate of variation with respect to Z of $\mathbf{u}$ (and P) as compared with transverse variations, terms involving $\partial/\partial Z$ can safely be ignored except when they are multiplied by the large quantity Ω. Thus

$$\frac{\partial \zeta}{\partial t} + (\mathbf{u}_1.\nabla_1)\,\zeta - \nu \nabla_1^2 \zeta \doteq 2\Omega \frac{\partial w}{\partial Z}, \tag{2.8}$$

where $w \equiv (\mathbf{u})_Z$, $\mathbf{u}_1 \equiv \mathbf{u} - \mathbf{k}w$ and $\nabla_1 \equiv \nabla - \mathbf{k}\,\partial/\partial Z$, $\mathbf{k}$ being a unit vector parallel to the Z axis. On imposing the appropriate boundary conditions at $Z = Z_l$ and

$Z = Z_u$, taking into account Ekman boundary layers of thickness $(\nu/\boldsymbol{\Omega}.\mathbf{n})^{\frac{1}{2}}$ ($\mathbf{n}$ being the local unit normal to the bounding surface), it may be shown that

$$\frac{\partial\bar{\zeta}}{\partial t}+(\mathbf{u}_1.\nabla_1)\,\bar{\zeta}=\frac{2\Omega}{Z_u-Z_l}\left\{-\left(\frac{\nu}{\Omega}\right)^{\frac{1}{2}}\bar{\zeta}+\mathbf{u}_1.\nabla_1(Z_u-Z_l)\right\}+\nu\nabla_1^2\bar{\zeta} \tag{2.9}$$

(see Hide 1968). According to (2.9), two processes bring about changes in vorticity of a moving filament: lateral friction, represented by the term $\nu\nabla_1^2\bar{\zeta}$, and stretching due to Ekman layer suction and transverse variations of (Z_u-Z_l), represented by the other terms on the right-hand side.

Previous work

The original work of Proudman (1916) and Taylor (1923) gave rise to a number of investigations of the effects of rapid rotation on fluid flow past solid objects, transverse motion, the case of interest here, having been discussed by Grace (1927), Stewartson (1953), Hide (1961, 1963, 1966), Jacobs (1964), Hide & Ibbetson (1966), Lighthill (1966, 1967), and Titman (1967), (and axial motion by Taylor (1922), Morgan (1951), Stewartson (1952, 1953, 1958), Long (1953), Lighthill (1967), Bretherton (1967), Drazin, Moore and Maxworthy, see Bretherton *et al.* (1966)).

Each theoretical study is characterized by the nature of the ageostrophic effects taken into account and whether the fluid is bounded or unbounded in the Z-direction. Thus, Stewartson (1953) and Lighthill (1967) treat unbounded systems when $\epsilon \neq 0$ and $\gamma = 0$, Hide (1961) (see also Hide & Ibbetson (1966)) treats a bounded system when $\epsilon \neq 0$ and $\gamma = 0$, and Jacobs (1964) treats a bounded system when $\gamma \neq 0$ and $\epsilon = 0$.

Stewartson (1953) (see also Grace (1927)) discusses the flow produced by jerking an ellipsoid impulsively from rest into steady motion, ageostrophic effects in his case being measured by the first term on the right-hand side of equation (2.6*b*), namely $(2\Omega\tau)^{-1}$. ζ satisfies the equation obtained by setting $(\mathbf{u}_1.\nabla_1)\zeta = \nu\nabla_1^2\zeta = 0$ in equation (2.8). Vorticity is generated at a (logarithmically) infinite rate within a region of infinitesimal volume at the surface of the ellipsoid, and remains constant in singular regions on that surface and within the wall of the Taylor column, where inertial oscillations persist indefinitely, even though the flow elsewhere becomes steady and irrotational ($\zeta = 0$) only a short time, of order $(2\Omega)^{-1}$ sec, after its initiation. $\langle\zeta\rangle$, the average value of $|\bar{\zeta}|$ over the disturbed region, depends on $\epsilon(Z_u-Z_l)/h$ and thus is indeterminate in Stewartson's problem.

Lighthill (1967, see also appendix below), who also deals with an unbounded system (see above), treats a steady Taylor column as a combination of inertial oscillations which, owing to the Doppler effect, appear to have zero frequency to an observer moving with the solid object. Ageostrophic effects in this case are measured by the second term on the right-hand side of (2.6*b*). On combining the equation obtained by setting $\partial\zeta/\partial t = \nu\nabla_1^2\zeta = 0$ in (2.8) with the third component of (2.5*b*) when $\gamma = 0$, it is readily shown (by inspection) that $\langle\zeta\rangle$ for the flows discussed by Lighthill is of order V/L.

Hide (1961), in proposing a theory of Jupiter's Great Red Spot, found it necessary to make a crude assessment of the effect of finite axial dimensions of the system on the conditions, as measured by ϵ, for pronounced Taylor columns to form, ϵ being the same as in Lighthill's problem, namely $V/L\Omega$ (see equation (2.6*b*)). Retaining only non-viscous terms in equation (2.9) and supposing that V/L is a rough upper limit to $\langle\zeta\rangle$, he argued from this equation that h, the amplitude of transverse variations in $(Z_u - Z_l)$, must exceed $\epsilon(Z_u - Z_l)$. (In a later paper Hide (1963) considers complications due to viscosity, density stratification and other factors that may arise in practice, especially in geophysical systems (see also Robinson (1960), Charney & Drazin (1961).)

Jacobs (1964), who ignores inertial effects altogether (see above), describes the steady flow around an isolated topographical feature, transverse dimensions L, of one rigid bounding surface of the fluid (the other rigid bounding surface being everywhere perpendicular to $\boldsymbol{\Omega}$). Viscous ageostrophic effects are concentrated in Ekman boundary layers of thickness $(\nu/\boldsymbol{\Omega}.\mathbf{n})^{\frac{1}{2}}$ and in a detached shear layer of thickness $(Z_u - Z_l)^{\frac{1}{2}}\nu^{\frac{1}{4}}/\sqrt{2}\,\Omega^{\frac{1}{4}}$ (the Stewartson (1957) thickness, assumed to be much less than L) that forms the wall of the Taylor column. Neglect of inertial effects is a valid procedure here when $\epsilon \ll \gamma^{\frac{1}{2}}$ (a condition that is hard to achieve in practice).

In Jacobs's work, both terms on the left-hand side of (2.9) are set equal to zero. Then $\mathbf{u}_1$ is such that filaments exactly follow those contours in planes perpendicular to $\boldsymbol{\Omega}$ on which $(Z_u - Z_l)$ remains constant, and w and $\bar{\zeta}$ vanish everywhere except in the wall of the Taylor column. Within this wall, where the two viscous terms on the right-hand side of (2.9) balance one another, $|\bar{\zeta}|$ attains a high value, of order $V/[(Z_u - Z_l)^{\frac{1}{2}}\nu^{\frac{1}{4}}/\sqrt{2}\,\Omega^{\frac{1}{4}}]$. However, $\langle\zeta\rangle$, the corresponding average value of $|\bar{\zeta}|$ over the whole of the Taylor column, is only V/L, as in Hide's case and Lighthill's case.

The original demonstration of the tendency for Taylor columns to form, an experiment for which γ and ϵ are not known, was made by rendering visible the streamlines of flow produced by towing a short cylinder of height and diameter equal to $0{\cdot}25D$ across the floor of a cylindrical, water-filled tank of depth D (Taylor 1923). One of the experiments of Hide & Ibbetson (1966) involved repeating and extending Taylor's work over ranges of ϵ and γ of $2{\cdot}7 \times 10^{-3}$ to $0{\cdot}16$ and $1{\cdot}6 \times 10^{-4}$ to $1{\cdot}8 \times 10^{-2}$ respectively. The observed flow patterns in planes perpendicular to $\boldsymbol{\Omega}$ were remarkably similar in general form to those predicted by Stewartson (1953), suggesting that viscous Ekman layers on the bounding surfaces in the experiment may permit axial motions to occur even in the geostrophic part of the Taylor column. (By (2·5*b*), when $\gamma = 0$ such axial motions can only occur when $(Z_u - Z_l)$ is infinite, as in Stewartson's case.)

Taylor columns over depressions as well as bumps in the bounding surfaces of the container of a rapidly rotating fluid have been demonstrated qualitatively by Hide (1966), Titman (1967), and in several unpublished studies, relative motion between the fluid and the container being generated either by varying the angular velocity of rotation of the container or by passing fluid slowly through the container by means of a suitable source–sink arrangement. (We chose the latter method for the experiments described below.)

3. Apparatus and techniques

(*a*) *Principles of operation of apparatus*

Figure 1 illustrates the relative flow in the apparatus. This flow, Eulerian velocity $\mathbf{u} = \mathbf{U}$ in the absence of the obstacle, was produced by withdrawing liquid at the rate $|Q|$ cc/sec at the rim or centre of a rotating cylindrical vessel and replacing it near the centre or rim at the same rate. Denote by D the depth of the tank, and by R_o and R_i the radii of curvature of the outer and inner concentric cylindrical side-walls.

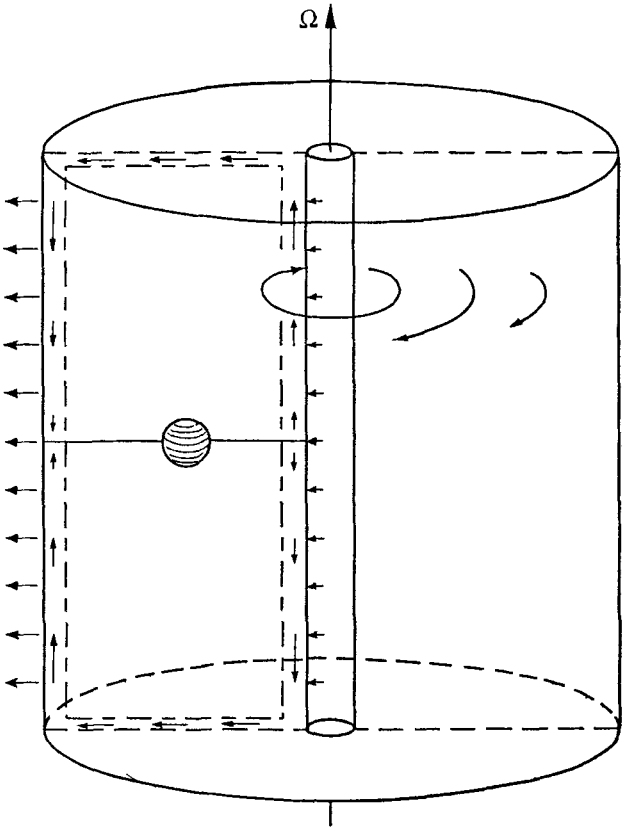

FIGURE 1. Schematic diagram of apparatus, drawn for the case $Q > 0$, so that $U_\vartheta < 0$.

The Ekman number (based on the length D) and the Rossby number (based on the length $(R_o - R_i)$) of the apparatus, respectively,

$$E \equiv \frac{\nu}{2\Omega D^2}, \quad F \equiv \frac{|Q|}{2\pi\nu^{\frac{1}{2}}\Omega^{\frac{1}{2}}(R_0^2 - R_i^2)}, \tag{3.1}$$

were always much less than unity. In these circumstances, the theory of the flow is best considered by splitting the meridional cross-section into five regions: the interior region, the boundary layer on the rigid impermeable end walls near

$Z = -\frac{1}{2}D$ and $Z = \frac{1}{2}D$, and the boundary layers on the source and on the sink, near $R = R_i$ and $R = R_o$ (see Hide 1968, especially figure 5).

It may be shown (see Hide 1968) that in the interior region

$$\mathbf{U} = (0, -Q\Omega^{\frac{1}{2}}/2\pi R\nu^{\frac{1}{2}}, 0), \quad \nabla \times \mathbf{U} = 0 \tag{3.2}$$

to zeroth order in $(E+F)$, the negative sign implying that the relative zonal flow is negative ('westward') or positive ('eastward') according as fluid is withdrawn at the rim or at the centre of the tank, Q being regarded as positive in the former case and negative in the latter. $\mathbf{U}$ has both radial and azimuthal components in the viscous Ekman layers, 95 % thickness 3δ, that occur on the end walls (see figure 1), where

$$\delta \equiv (\nu/\Omega)^{\frac{1}{2}} \tag{3.3}$$

and typically much less than D. $\mathbf{U}$ has radial, azimuthal and axial components in the side-wall boundary layers of thickness Δ_{in} (for the source) and Δ_{out} (for the sink) where

$$\Delta_{in} \doteq \frac{3D^{\frac{1}{2}}\delta^{\frac{1}{2}}}{\sqrt{2}} f_{in}(E, F, R_o/R_i), \quad \Delta_{out} \doteq \frac{3D^{\frac{1}{2}}\delta^{\frac{1}{2}}}{\sqrt{2}} f_{out}(E, F, R_o/R_i). \tag{3.4}$$

Conservative lower limits to Δ_{in} and Δ_{out} may be obtained by considering the case when fluid enters or leaves the system uniformly over the cylindrical surfaces of the source and sink. Then

$$f_{in} \doteq (1 + \tfrac{1}{4}X^2)^{\frac{1}{2}} + \tfrac{1}{2}X, \quad f_{out} \doteq (1 + \tfrac{1}{4}X^2)^{\frac{1}{2}} - \tfrac{1}{2}X, \tag{3.5}$$

where

$$X \equiv \frac{|Q|}{6\pi\sqrt{2}\, R_{o,i}\nu^{\frac{1}{4}}\Omega^{\frac{1}{4}}D^{\frac{1}{2}}} = \frac{F(R_o^2 - R_i^2)}{3 \times 2^{\frac{1}{4}}E^{\frac{1}{4}}DR_{o,i}} \tag{3.6}$$

and $R_{o,i}$ is the radius of curvature of the surface of the source or sink, R_o or R_i as the case may be (Hide 1968). The actual values of Δ_{in} and Δ_{out} should not greatly exceed these lower limits, although no one has treated the theory of the effect on these quantities of local variations in strength over the surface of the source or sink except when $X \ll 1$, in which case the values of f given by equation (3.5) are too low by about $E^{-\frac{1}{12}}$.

The useful range of parameters over which it can safely be assumed that U_ϑ, the ϑ component of $\mathbf{U}$, varies inversely with R within the region $|Z| < (\frac{1}{2}D - 3\delta)$, $(R_i + \Delta_{in}) < R < (R_o - \Delta_{out})$ (when $Q > 0$) is limited by the occurrence of various kinds of instabilities. As the investigation of these instabilities is far from complete (Hide 1968), it was necessary to ascertain the suitability of any given combination of experimental parameters by means of calibration experiments (see below). A safe rule is to keep the Reynolds number based on δ,

$$|Q|/2\pi\nu R_i = F(R_o^2 - R_i^2)/\sqrt{2}\, E^{\frac{1}{2}}DR_i,$$

as small as possible; Ekman layer instabilities certainly occur when this parameter attains values as high as 50 and may occur at even lower values. The side-wall boundary layers are known to exhibit instabilities even when the Ekman layer is quite stable.

(*b*) *Construction of apparatus and techniques of observation and measurement*

The apparatus used in the experiments was that used previously in unpublished work on Taylor columns by Hide and Greenfield, but with slight modifications. It consisted of a circular tank, 29·2 cm internal diameter, 30·9 cm internal depth, fitted with a removable lid. Liquid could be introduced into the tank through a small (0·25 mm) annular gap between the upper lid and the outer wall; it was removed from the tank through an axial tube of outer radius $R_i = 0{\cdot}5$ cm which had small perforations along its length. The flow from the centre of the tank to

Parameter	Value
D (cm)	30·9
R_i (cm)	0·5
R_o (cm)	14·6
$\bar{R}$ (cm)	7·3
h (cm)	2·54
L (cm)	2·54
Ω (rad/sec)	2·10
$\|Q\|$ (cc/sec)	$6{\cdot}95 \times 10^{-2}$ to 3·83
$\|Q\|$ (cc/sec) (range covered by calibration experiments)	$2{\cdot}24 \times 10^{-1}$ to 3·78
ν (cm²/sec)	$0{\cdot}88 \times 10^{-2}$ to $14{\cdot}1 \times 10^{-2}$
$\delta \equiv (\nu/\Omega)^{\frac{1}{2}}$ (cm)	$6{\cdot}46 \times 10^{-2}$ to $2{\cdot}64 \times 10^{-1}$
$\|Q\|/2\pi D\bar{R}$ (cm/sec)	$4{\cdot}93 \times 10^{-5}$ to $2{\cdot}72 \times 10^{-3}$
$U_\vartheta(\bar{R}) = \|Q\|/2\pi\delta\bar{R}$ (cm/sec)	$1{\cdot}01 \times 10^{-2}$ to 1·26
$E \equiv \nu/2\Omega D^2$	$2{\cdot}19 \times 10^{-6}$ to $3{\cdot}40 \times 10^{-5}$
$F \equiv \|Q\|/2\pi\nu^{\frac{1}{2}}\Omega^{\frac{1}{2}}(R_o^2 - R_i^2)$	$1{\cdot}70 \times 10^{-4}$ to $2{\cdot}13 \times 10^{-2}$
$\|Q\|/2\pi\nu R_i$	$2{\cdot}72 \times 10^{-1}$ to 132
$\|Q\|/2\pi\nu\bar{R}$	$1{\cdot}86 \times 10^{-2}$ to 9·06
$\|Q\|/2\pi\nu D$	$4{\cdot}40 \times 10^{-3}$ to 2·14
$\gamma \equiv 2\nu/L^2\Omega$	$1{\cdot}30 \times 10^{-3}$ to $2{\cdot}03 \times 10^{-2}$
$\epsilon \equiv \|Q\|/2\pi\delta\Omega\bar{R}L$	$1{\cdot}89 \times 10^{-3}$ to $2{\cdot}36 \times 10^{-1}$
$\epsilon D/h$	$2{\cdot}30 \times 10^{-2}$ to 2·87

TABLE 1. Range of experimental parameters

the rim was maintained externally by a centrifugal pump. The flow rate through the circuit was adjusted using a needle valve, and was measured by means of a 'Manostat' flowmeter. Small perturbations in the pump pressure were damped out using an 'R-C' filter consisting of a long open vertical tube of large diameter (capacitor) coupled into the flow circuit just before the needle valve constriction (resistor). Pressure fluctuations at the pump thus produced small changes in level in the capacitor tube rather than variations in flow rate through the circuit. The tank and pumping equipment were fixed to a rotating table capable of rotation at steady speeds up to 10 rad/sec. The experimental parameters are listed in table 1.

Fluid motions in the tank were rendered visible by releasing dye electrolytically from thin (0·36 mm diameter) wires strung radially across the tank. The

liquid in the tank, either water or an aqueous sucrose solution, contained a dilute (0·01 %, w/w) solution of thymol blue indicator, normally light amber in colour, which had been titrated almost to the end-point using sodium hydroxide solution. When a potential difference of up to 40 V was applied across the electrodes in the tank, the local increase in concentration of hydroxyl ions at the anode was sufficient to cause the solution there to change colour to its dark blue, basic form. The blue solution was swept from the wire by the flow, reverting slowly to its acidic amber colour some distance downstream of the wire after diffusion had restored the local pH value to normal. Because the specific gravity of the dye was equal to that of the working liquid, spurious effects due to buoyancy forces were avoided, an obvious advantage over methods employing dyes that are not neutrally buoyant (see Baker 1966). Another advantage of the method is that the solution may be used indefinitely, never needing replenishment.

Photographs of the flow patterns were taken with a 35 mm camera capable of remote electrical operation and mounted on the turntable.

(*c*) *Calibration experiments*

Before conducting the experiments on the flow past obstacles, it was necessary to ascertain the extent to which the basic 'interior' flow in the tank corresponded to the theoretical steady-state geostrophic value given by (3.2). Calibration experiments were therefore carried out without an obstacle in the tank.

The flow was measured at only one depth in the tank. Dye was released from points at 1·5 cm intervals along a wire stretched radially across the annulus midway between the top and the bottom. The dye was released periodically by interrupting the electrode circuit with a micro-switch actuated by a cam on a timing motor. The interruption rate was adjusted so as to give a reasonable separation between successive dye streaks at all radii for a given flow rate. Photographs of the dye streaks were then obtained over almost as wide a range of flow rates as would be used in the main experiments. The photographs showed concentric sets of dye streaks, the azimuthal separation of the streaks at one radius being proportional to U_ϑ, the ϑ component of $\mathbf{U}$. $U_\vartheta(R)$ was determined from measurements of the separation of the dye streaks and the interruption frequency.

The results of the calibration experiments are shown in figure 2. Here, the observed values of the quantity RU_ϑ are plotted as a function of R. Theoretically, (see equation (3.2)), RU_ϑ should equal $-Q/2\pi\delta$ (indicated on the right-hand side of the graph for each experiment) outside the boundary layers. If we take as the boundary layer the region where the ratio $|RU_\vartheta/(Q/2\pi\delta)|$ is less than 95 %, according to figure 2 the boundary-layer thickness at the outer wall is about 3 cm, while that at the inner wall is about 4 cm (although there are fewer measurements there). The 'interior' of the fluid thus extends about 3·5 cm on either side of a mean radius of about 7·5 cm in the annulus.

These calibration experiments showed (i) that over the range of conditions studied (see figure 2) the flow in the 'interior' of the annulus was geostrophic (and therefore two-dimensional) to within the accuracy of the calibration experiments

(± 5 % overall) and (ii) that the radial dimensions of the 'interior' region were about 7 cm, presumably sufficient for the performance of Taylor column experiments using an obstacle of width not greater than 3 cm centred at $R = \bar{R} = 7{\cdot}3$ cm.

4. Flow past a sphere at constant Ekman number

In the first experiment the obstacle was a sphere of diameter

$$2a = h = L = 2{\cdot}54\,\text{cm}$$

(see table 1). It was held fixed in position relative to the annular tank, with its centre 7·3 cm from the axis of the tank and exactly midway between the end-

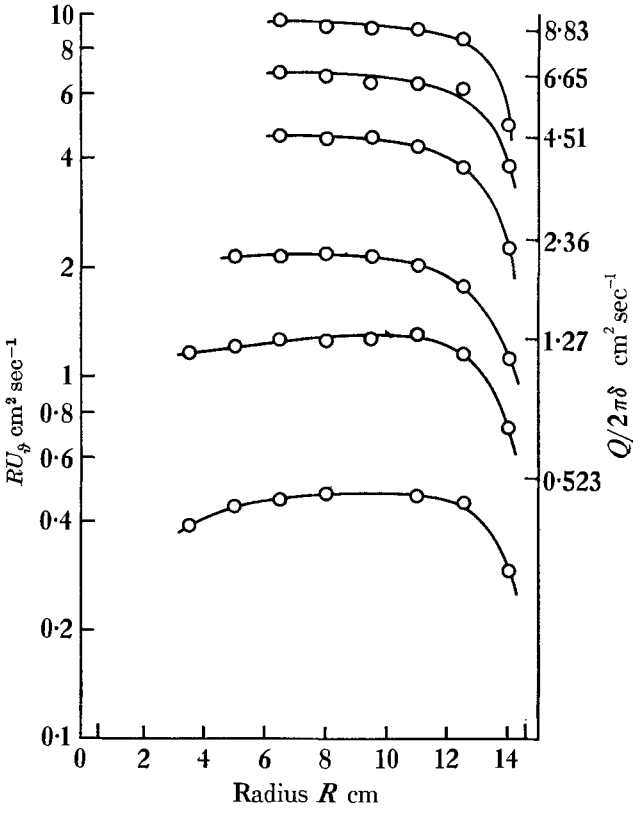

FIGURE 2. Results of calibration experiments. RU_ϑ is plotted as a function of R; in the interior region, RU_ϑ should be a constant whose value, $Q/2\pi\delta$, is indicated on the right-hand side of the graph for each experiment.

walls, by means of a thin, rigid wire (diameter 0·1 cm) stretched along the radius of the tank in $Z = 0$ that passed through the centre of the sphere, azimuthal co-ordinate $\vartheta = \bar{\vartheta}$. Water was the fluid in the tank.

In this experiment Q was negative, so that U_ϑ was positive (see equation (3·2)). Stream surfaces of the flow over the sphere were made visible by continuously releasing blue dye at the horizontal wires stretched across the annulus at $\vartheta = \bar{\vartheta} - 22°$, $Z = Z_s = 1{\cdot}1$, 2·9, 5·0, 7·2, 9·2, 11·1 and 12·9 cm. Photographs were

obtained showing the distortion due to the presence of the sphere of the initially horizontal stream surfaces. Figure 3, plates 1 to 3, shows three examples, corresponding to different values of ϵ, of the appearance of the dye surfaces when looking towards the axis of the tank along the radius on which the sphere was fixed; hence, Z increases upwards and ϑ from left to right. Figure 4*a*, plate 4, shows one example of the appearance of the dye surfaces looking into the tank at right angles to the radius through the centre of the sphere in the negative ϑ direction from downstream of the sphere; hence Z increases upwards and R from right to left. Figure 4*b*, plates 4 and 5, illustrates the distortion of a line of dye released from a wire upstream of the spherical obstacle looking at right angles to the radius through the sphere in a direction parallel to the negative Z axis. It should be emphasized that in figures 3*a–c* and figure 4*a* the appearance of the dyed stream surfaces was independent of time: in each case the distribution of dye had reached a steady state before the photograph was taken.

Denote by $\mathfrak{Z}(R, \vartheta, Z_s)$ the axial displacement directed away from the plane $Z = 0$ of a dyed stream-surface which, in the absence of the sphere, would occupy the plane $Z = Z_s$. Denote by $(R_m(Z_s), \vartheta_m(Z_s))$ the radial and azimuthal co-ordinates of the point where $\mathfrak{Z}$ has its maximum value, $\mathfrak{Z}_m(Z_s)$, on that distorted dyed stream-surface whose undisturbed equation is $Z = Z_s$.

According to figures 3 and 4, $\mathfrak{Z}$ is positive above most of the sphere, but negative over a small region (to the left of the sphere as seen in figure 4*a*, and in the foreground and slightly downstream of the sphere in figure 3).

For the conditions illustrated by figure 4*a*, R_m, the radial co-ordinate of the position of maximum $\mathfrak{Z}$, was slightly less than $\bar{R}$, the radial co-ordinate of the centre of the sphere. A subsidiary investigation, involving changing the sign of Q and the sense of rotation of the apparatus, showed that the sign of $(R_m - \bar{R})$ is the same as that of the radial component of $\mathbf{\Omega} \times \mathbf{U}$ (so that the slight radial displacement of the Taylor column is in the direction of high to low (dynamic) pressure associated with the basic current) and demonstrated that this displacement is *not* connected with the sense of shear or curvature of the streamlines of the basic flow.

Returning now to the experiments illustrated by figures 3 and 4, it would seem that $\mathfrak{Z}_m$ decreases slowly with Z_s (cf. figures 3*a*, *b* and *c*). The same figures show that $(\vartheta_m - \bar{\vartheta})$ is positive and increases with Z_s, corresponding to a downstream 'trailing' of the Taylor column. Moreover, the rate of increase of $(\vartheta_m - \bar{\vartheta})$ with Z_s is most pronounced at the highest values of ϵ (see figure 3).

From photographs similar to those presented in figure 3, taken at 17 different values of ϵ, ranging from $4{\cdot}32 \times 10^{-3}$ to 0·236 (γ being kept constant at $1{\cdot}36 \times 10^{-3}$, see table 1 and equations (1.1)), the determinations of $\mathfrak{Z}_m$ presented in table 2 were obtained. For 9 of these values of ϵ, ranging from $1{\cdot}38 \times 10^{-2}$ to 0·236, $(\vartheta_m - \bar{\vartheta})$, though small, was also measureable (see table 2). In making these determinations it was necessary to correct for optical distortions of the photographic images. These distortions were due to refraction effects in the cylindrical tank, which magnified distances in the azimuthal direction by a factor 1·18, and in the vertical direction by a factor 1·06.

The measurements of Z_s, $\mathfrak{Z}_m(Z_s)$ and $R_m(\vartheta_m - \bar{\vartheta})$ from the photographs were

Z_s (cm)	$R_m(\vartheta_m-\overline{\vartheta})$ (cm)	$\mathfrak{Z}_m$ (cm)	$R_m(\vartheta_m-\overline{\vartheta})$ (cm)	$\mathfrak{Z}_m$ (cm)	$R_m(\vartheta_m-\overline{\vartheta})$ (cm)	$\mathfrak{Z}_m$ (cm)
ϵ	$2{\cdot}36\times10^{-1}$		$2{\cdot}05\times10^{-1}$		$1{\cdot}76\times10^{-1}$	
1·1	0·80	1·2	0·69	1·2	0·63	1·3
2·9	1·67	1·1	1·38	1·1	1·33	1·2
5·0	2·02	0·8	1·78	0·9	1·72	0·9
7·2	2·64	0·5	2·30	0·6	2·19	0·6
9·2	3·11	0·3	2·76	0·4	2·53	0·4
11·1	—	—	—	—	—	—
12·9	—	—	—	—	—	—
ϵ	$1{\cdot}47\times10^{-1}$		$1{\cdot}19\times10^{-1}$		$8{\cdot}95\times10^{-2}$	
1·1	0·51	1·3	0·41	1·3	0·29	1·3
2·9	1·04	1·2	0·80	1·2	0·63	1·3
5·0	1·38	0·9	1·15	1·0	0·80	1·0
7·2	1·96	0·7	1·50	0·7	1·21	0·7
9·2	2·13	0·4	1·72	0·5	1·33	0·6
11·1	2·42	0·3	2·19	0·3	1·55	0·4
12·9	—	—	—	—	1·67	0·2
ϵ	$6{\cdot}23\times10^{-2}$		$3{\cdot}36\times10^{-2}$		$1{\cdot}38\times10^{-2}$	
1·1	0·17	1·3	0	1·2	0	1·2
2·9	0·35	1·3	0·12	1·2	0	1·1
5·0	0·51	1·0	0·17	1·0	0	0·8
7·2	0·75	0·8	0·29	0·7	0·06	0·5
9·2	0·86	0·6	0·41	0·5	0·06	0·4
11·1	1·09	0·4	0·46	0·4	0·17	0·4
12·9	1·09	0·3	0·51	0·3	0·12	0·3
ϵ	$1{\cdot}06\times10^{-2}$		$9{\cdot}95\times10^{-3}$		$9{\cdot}01\times10^{-3}$	
1·1	0	1·2	0	1·4	0	1·1
2·9	0	1·0	0	1·1	0	0·9
5·0	0	0·9	0	0·9	0	0·8
7·2	0	0·8	0	0·7	0	0·7
9·2	0	0·6	—	—	0	0·6
11·1	0	—	—	—	—	—
12·9	—	—	—	—	—	—
ϵ	$7{\cdot}41\times10^{-3}$		$6{\cdot}68\times10^{-3}$		$5{\cdot}78\times10^{-3}$	
1·1	0	1·2	0	1·0	0	1·1
2·9	0	1·0	0	0·8	0	0·9
5·0	0	0·9	0	0·7	0	0·7
7·2	0	0·8	0	0·5	0	0·6
9·2	0	0·6	0	0·4	0	0·4
11·1	—	—	—	—	—	—
12·9	—	—	—	—	—	—
ϵ	$5{\cdot}10\times10^{-3}$		$4{\cdot}32\times10^{-3}$			
1·1	0	0·8	0	0·7		
2·9	0	0·6	0	0·5		
5·0	0	0·5	0	0·45		
7·2	0	0·4	0	0·35		
9·2	0	0·3	0	0·25		
11·1	—	—	—	—		
12·9	—	—	—	—		

TABLE 2

each subject to an uncertainty of $\pm 0{\cdot}1$ cm. Measurements of ϵ involved uncertainties varying from about ± 2 % at large values of ϵ to about ± 5 % at small values; they were incurred in the determination of the flow rate Q by reading the flowmeter on the rotating table. The errors in measuring other parameters were estimated to be much less than 1 % in each case.

The experimentally determined variation of $R_m(\vartheta_m - \overline{\vartheta})$ with Z_s (see table 2) for each value of ϵ is well represented by the empirical relationship

$$R_m(\vartheta_m - \overline{\vartheta}) = Z_s \tan\psi \tag{4.1}$$

except in the two cases $\epsilon = 3{\cdot}36 \times 10^{-2}$ and $\epsilon = 1{\cdot}38 \times 10^{-2}$, where the data suggest a roughly hyperbolic variation whose asymptote satisfies (4.1). The values of $\tan\psi$ thus determined for different values of ϵ, together with estimated

$\tan\psi$	ϵ
$0{\cdot}356 \pm 0{\cdot}016$	$2{\cdot}36 \times 10^{-1}$
$0{\cdot}305 \pm 0{\cdot}007$	$2{\cdot}05 \times 10^{-1}$
$0{\cdot}278 \pm 0{\cdot}008$	$1{\cdot}76 \times 10^{-1}$
$0{\cdot}238 \pm 0{\cdot}010$	$1{\cdot}47 \times 10^{-1}$
$0{\cdot}187 \pm 0{\cdot}005$	$1{\cdot}19 \times 10^{-1}$
$0{\cdot}143 \pm 0{\cdot}005$	$8{\cdot}95 \times 10^{-2}$
$0{\cdot}097 \pm 0{\cdot}004$	$6{\cdot}23 \times 10^{-2}$
$0{\cdot}047 \pm 0{\cdot}004$	$3{\cdot}36 \times 10^{-2}$
$0{\cdot}018 \pm 0{\cdot}003$	$1{\cdot}38 \times 10^{-2}$
Also: $D = 30{\cdot}9$ cm	$2a = h = L = 2{\cdot}54$ cm
$R_i = 0{\cdot}5$ cm	$R_o = 14{\cdot}6$ cm
$\Omega = 2{\cdot}10$ rad/sec	$\nu = 0{\cdot}92 \times 10^{-2}$ cm^2/sec
$Q < 0$	$\gamma = 1{\cdot}36 \times 10^{-3}$

TABLE 3

errors, are given in table 3 and plotted in figure 5. It is clear from figure 5 that the data are well represented by a linear relationship,

$$\tan\psi = K\epsilon, \tag{4.2}$$

where, by a least-squares analysis,

$$K = 1{\cdot}54 \pm 0{\cdot}04 \quad \text{(standard error, 9 points)} \tag{4.3}$$

(cf. equation (1.3)).

The foregoing results agree with Lighthill's conclusions that Taylor columns should trail at an angle of the order of the Rossby number to the Z axis (see appendix). Moreover, within the (small) errors of measurement, the measured value of K does not differ significantly from Lighthill's theoretical value. This agreement between experiment and theory is remarkable, considering the simplifications of the theory, which treats the flow field at great distances from a sphere in an unbounded, inviscid fluid.

Table 2 shows that in the experiment just described, the variation of $\mathfrak{Z}_m$ with Z_s does not depend significantly on ϵ. We shall defer the discussion of this variation until § 6, where it is shown, by studying the effects of viscosity on the flow patterns just described, that $d\mathfrak{Z}_m/dZ$ depends mainly on γ, the Ekman number.

5. Transverse flow past a cylinder at constant Ekman number

Figure 6, plates 6 and 7, illustrates observations of flow past a right circular cylinder, $h = 2{\cdot}54$ cm, $L = 2{\cdot}54$ cm, obtained in the same way as those of flow past a sphere described above in § 4 (cf. figures 3 and 4), for one value of ϵ, namely $9{\cdot}1 \times 10^{-3}$, typical of the range of ϵ studied.

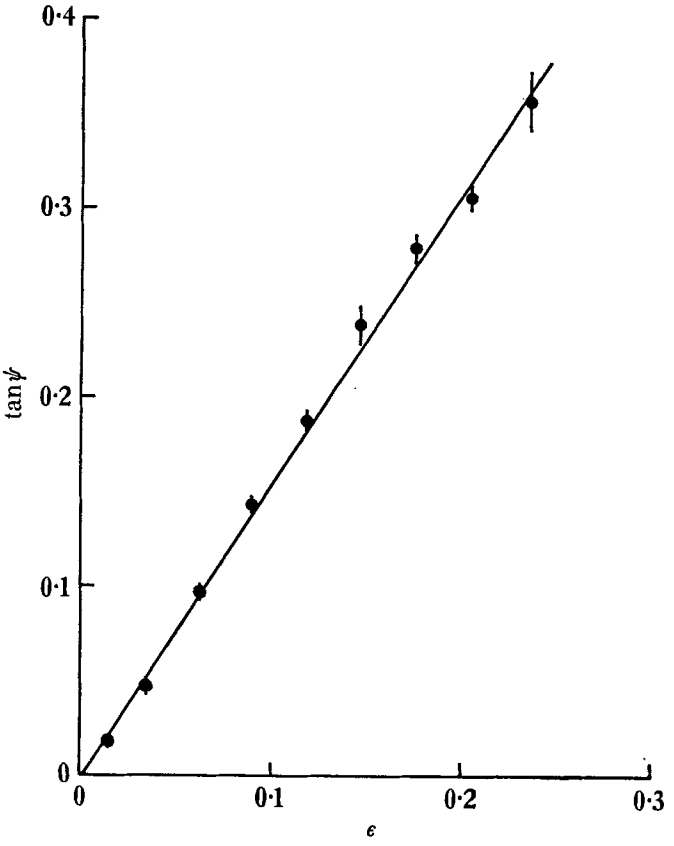

FIGURE 5. Graph of tan ψ versus ϵ for the sphere. $\gamma = 1{\cdot}36 \times 10^{-3}$.

Although figures 6*c* show a distinct tendency for a Taylor column to form, figures 6*a* and *b* show that the flow pattern was more complicated than in the case of a sphere. As in that case, the sign of $(R_m - \bar{R})$, the displacement of the position of maximum $\mathcal{J}$, was the same as the sign of the radial component of $\boldsymbol{\Omega} \times \mathbf{U}$ (see figure 6*b*), and negative values of $\mathcal{J}$ were found on the other side of the axis of the cylinder. Owing to the complexity of these patterns, no attempt was made to carry out an extensive series of measurements (cf. § 4). This complexity was due, presumably, to the abrupt changes in slope associated with the walls of the cylinder (cf. equation (2.9)).

6. Transverse flow past a sphere: effect of increasing the viscosity

The experimental results described in § 4 and listed in table 2 show that, at any given value of ϵ, $\mathfrak{Z}_m$, the maximum amplitude of the axial distortion of the stream surface originally at a distance $Z = Z_s$ from the plane $Z = 0$, decreases with increasing Z_s. That this decrease is linear, of the form

$$\mathfrak{Z}_m(Z_s) = \mathfrak{Z}_m(0)\,[1 - Z_s/Z_c], \tag{6.1}$$

where $\mathfrak{Z}_m(0)$ and Z_c are constants for given ϵ and γ, is consistent with the experimental measurements (see table 2).

γ	ϵ	$\mathfrak{Z}_m(0)$ (cm)	Z_c (cm)
	(*a*)		
$1{\cdot}36 \times 10^{-3}$	$2{\cdot}36 \times 10^{-1}$	1·38	11·8
	$2{\cdot}05 \times 10^{-1}$	1·36	13·2
	$1{\cdot}76 \times 10^{-1}$	1·48	12·6
	$1{\cdot}47 \times 10^{-1}$	1·45	13·6
	$1{\cdot}19 \times 10^{-1}$	1·47	14·1
	$8{\cdot}95 \times 10^{-2}$	1·48	15·0
	$6{\cdot}23 \times 10^{-2}$	1·47	15·8
	$3{\cdot}36 \times 10^{-2}$	1·36	15·8
	$1{\cdot}38 \times 10^{-2}$	1·24	15·3
	$1{\cdot}06 \times 10^{-2}$	1·25	18·3
	$9{\cdot}95 \times 10^{-3}$	1·48	13·2
	$9{\cdot}01 \times 10^{-3}$	1·12	19·2
	$7{\cdot}41 \times 10^{-3}$	1·25	18·3
	$6{\cdot}68 \times 10^{-3}$	1·05	14·4
	$5{\cdot}78 \times 10^{-3}$	1·16	14·0
	$5{\cdot}10 \times 10^{-3}$	0·82	14·0
	$4{\cdot}32 \times 10^{-3}$	0·71	13·9
		1·27 mean	14·8 mean
	(*b*)		
$1{\cdot}30 \times 10^{-3}$	$2{\cdot}42 \times 10^{-2}$	1·28	19·0
$5{\cdot}65 \times 10^{-3}$	$1{\cdot}12 \times 10^{-2}$	1·33	11·4
$2{\cdot}01 \times 10^{-2}$	$6{\cdot}04 \times 10^{-3}$	1·49	7·9
$2{\cdot}01 \times 10^{-2}$	$1{\cdot}89 \times 10^{-3}$	1·32	8·0
		1·35 mean	

TABLE 4

The variation of $\mathfrak{Z}_m(0)$ and Z_c with ϵ for one value of γ, namely $1{\cdot}36 \times 10^{-3}$, is shown in table 4*a*. Evidently Z_c varies very slowly, if at all, with ϵ, and, with the possible exception of the cases when $\epsilon > 0{\cdot}15$, we may take $Z_c = (14{\cdot}8 \pm 0{\cdot}5)$ cm and independent of ϵ. It is also noteworthy that the mean of the 17 values of $\mathfrak{Z}_m(0)$ given in table 4*a* is exactly equal to the radius of the sphere, 1·27 cm, although the spread of values about the mean is quite large.

The dependence of Z_c on γ was investigated by repeating the procedure described in § 4 but using aqueous solutions of sucrose instead of water as the working fluid. (The kinematical viscosity of these solutions was determined by means of a Fenske Routine Viscometer, which involved measuring the time taken

for a known volume of liquid to flow through a capillary tube past a fiduciary mark, small temperature corrections being estimated by interpolation from tables (*Handbook of Chemistry and Physics*, 1963)). As before, photographs of dye produced by radial wires upstream of the sphere were obtained, and $\mathfrak{Z}_m$ at each value of Z_s was tabulated for each photograph (see table 5). It was not possible to hold ϵ constant in these experiments, but in view of the lack of dependence of Z_c on ϵ found earlier, this difficulty was probably not serious.

ν (cm²/sec)	$8{\cdot}84\times10^{-3}$	$3{\cdot}82\times10^{-2}$	$1{\cdot}37\times10^{-1}$	$1{\cdot}37\times10^{-1}$
E	$2{\cdot}17\times10^{-6}$	$0{\cdot}96\times10^{-5}$	$3{\cdot}40\times10^{-5}$	$3{\cdot}40\times10^{-5}$
γ	$1{\cdot}30\times10^{-3}$	$5{\cdot}65\times10^{-3}$	$2{\cdot}01\times10^{-2}$	$2{\cdot}01\times10^{-2}$
ϵ	$2{\cdot}42\times10^{-2}$	$1{\cdot}12\times10^{-2}$	$6{\cdot}04\times10^{-3}$	$1{\cdot}89\times10^{-3}$
Z_s (cm)	$\mathfrak{Z}_m$ (cm)	$\mathfrak{Z}_m$ (cm)	$\mathfrak{Z}_m$ (cm)	$\mathfrak{Z}_m$ (cm)
1·1	1·3	1·3	1·4	1·2
2·9	1·0	0·9	0·8	0·8
5·0	0·9	0·7	0·5	0·4
7·2	0·8	0·5	0·2	0·2
9·2	0·7	0·3	—	—

TABLE 5

ν (cm²/sec)	Z_c (cm)	γ	$Z_c\gamma^{\frac{1}{4}}/L$	$Z_c\gamma^{\frac{1}{2}}/L$
$9{\cdot}28\times10^{-3}$	$14{\cdot}8\pm0{\cdot}5$*	$1{\cdot}36\times10^{-3}$	$1{\cdot}14\pm0{\cdot}04$	$0{\cdot}22\pm0{\cdot}01$
$8{\cdot}84\times10^{-3}$	$19{\cdot}0\pm3{\cdot}6$†	$1{\cdot}30\times10^{-3}$	$1{\cdot}39\pm0{\cdot}26$	$0{\cdot}27\pm0{\cdot}05$
$3{\cdot}82\times10^{-2}$	$11{\cdot}4\pm1{\cdot}4$†	$5{\cdot}65\times10^{-3}$	$1{\cdot}24\pm0{\cdot}15$	$0{\cdot}34\pm0{\cdot}04$
$1{\cdot}37\times10^{-1}$	$7{\cdot}95\pm1{\cdot}0$†	$2{\cdot}01\times10^{-2}$	$1{\cdot}18\pm0{\cdot}15$	$0{\cdot}44\pm0{\cdot}06$

* Mean of 17 readings and standard error of mean; see table 4.
† Standard errors obtained from least squares calculation using data of table 5.
L = 2·54 cm and was not varied.

TABLE 6

Values of $\mathfrak{Z}_m(0)$ and Z_c based on table 5, assuming the validity of equation (6.1), are given in table 4*b*. While $\mathfrak{Z}_m(0)$ is more or less independent of γ and very nearly equal to the radius of the sphere, Z_c evidently decreases with increasing γ. Table 6 lists the mean value of Z_c for the experiments described in § 4 (see table 4*a*) and the three values of Z_c given in table 4*b*. Values of $Z_c\gamma^{\frac{1}{4}}/L$ and, for comparison, $Z_c\gamma^{\frac{1}{2}}/L$ are also shown. The apparent lack of systematic variation of $Z_c\gamma^{\frac{1}{4}}/L$ with γ, and the fact that this quantity is close to unity, suggests that Z_c might, in fact vary as $\gamma^{-\frac{1}{4}}$. This result is tentative, of course, and should be tested in the future by means of experiments covering a wider range of γ than that used in the present investigation. It will also be important in future work to attain values of $\frac{1}{2}D$ significantly in excess of L/ϵ, so that the dependence of Z_c on ϵ can be determined.

The extent to which Z_c can be regarded as a useful measure of the length of the Taylor column is not clear, in the absence of detailed knowledge of the relationship between $\mathfrak{Z}$ and the transverse field of motion. The experimental determina-

tion of this relationship—a lengthy though probably useful undertaking—lies beyond the scope of the present work.

If Z_c *can* be regarded as a useful measure of the length of the Taylor column, then the fact that Z_c depends on γ suggests that the Taylor column terminates when the thickness of a detached viscous shear layer that forms the wall of the column is equal to $\frac{1}{2}L$. If the thickness of this shear layer depends *only* on Z, ν and Ω, then it must vary as $Z^{(1-2q)}(\nu/\Omega)^q$ and if $Z_c \propto L\gamma^{-\frac{1}{4}}$, then $q = \frac{1}{6}$. In the strictly viscous case discussed by Jacobs (see § 2) the detached shear layer forming the wall of the Taylor column has the Stewartson thickness, for which $q = \frac{1}{4}$.

We thank Prof. M. J. Lighthill for contributing the appendix to this paper, and acknowledge that it was his review paper (see Lighthill 1966) at a symposium on the 'Dynamics of Rotating Fluids' held in April 1965 at La Jolla, California, by the International Union of Theoretical and Applied Mechanics that stimulated our interest in extending our earlier work on Taylor columns. We also thank Mr Robert Frazel for technical assistance.

Financial support was provided by the National Science Foundation under grant GP 5053 (Atmospheric Sciences Program) to the Massachusetts Institute of Technology and by the Office of Naval Research under grant 2196(00) to the Woods Hole Oceanographic Institution. This is paper number 24 of the Geophysical Fluid Dynamics Laboratory, Department of Geology and Geophysics, M.I.T.

Appendix. Theoretical considerations for the steady inviscid case with Rossby number small but not zero

By M. J. LIGHTHILL

This appendix sets out some theoretical considerations, for comparison with the experiments described in the paper, in cases when the transverse motion of the obstacle is steady, the Ekman number is negligibly small, and the Rossby number is small but not negligibly so.

Preliminary study of this problem for obstacles of general shape was given by Lighthill (1967), who started from the assumption that the disturbances cannot remain of 'Taylor column' character, or indeed of any unattenuated form, all the way to infinity. At sufficiently large distances from the obstacle, he argued, they must become weak, and therefore must take the form of stationary inertial waves; essentially, because inertial waves are the only possible form of small disturbance to a homogeneous rotating fluid, and because waves in flow that is steady (relative to the obstacle) must be stationary.

Lighthill (1967) obtained results on the possible distribution of such waves that can be expressed as follows. If the obstacle moves with velocity $(U, 0, 0)$ through fluid rotating with angular velocity $(0, 0, \Omega)$, then waves of wave-number

$$\left(\kappa\cos\phi,\ \kappa\sin\phi,\ \pm\frac{U\kappa^2}{2\Omega}\cos\phi\right), \tag{A 1}$$

where the z-component is necessarily related to the x- and y-components as shown (Lighthill 1967, equation (67)), are found in directions

$$\left(-\frac{U\kappa}{2\Omega}(\tfrac{3}{2}+\tfrac{1}{2}\cos 2\phi),\ -\frac{U\kappa}{2\Omega}(\tfrac{1}{2}\sin 2\phi),\ \pm 1\right) \tag{A 2}$$

relative to the position of the obstacle. Here the $\sqrt{(l^2+m^2)}$ in equation (71) of Lighthill (1967) has been replaced by κ, while his figure 11 shows that the choices of sign in (A 1) and (A 2) must be the same if $\cos\phi$ is positive and different if $\cos\phi$ is negative.

Obstacles moving at small Rossby number are expected to generate waves with κ small in relation to $2\Omega/U$ and so the axial component of wave-number, $\pm(U\kappa^2/2\Omega)\cos\phi$ in (A 1), is small compared with the radial component κ (which therefore is to close approximation the magnitude of the wave-number vector). This fact (which, actually, was used in deriving (A 2)) means that surfaces of constant phase for all the waves make small angles with the axis of rotation, and that waves are found only in directions (measured from the obstacle) close to that of the axis of rotation. Specifically, waves of length $2\pi/\kappa$ are found on two cones (swept out by the directions (A 2) as ϕ varies), each with axis trailing at an angle

$$\tfrac{3}{2}(U\kappa/2\Omega) \tag{A 3}$$

behind the axis of rotation, and with semi-angle $\frac{1}{2}(U\kappa/2\Omega)$.

Lighthill (1967) points out that a given obstacle will generate waves most of whose energy lies in a range of values of κ from 0 to some upper limit of the order of the reciprocal of a linear dimension of the obstacle. He indicates in his figure 12 how these waves would fill a region obtained by superimposing the cones just described for all values of κ in this range, and shows the sorts of shapes of surfaces of constant phase that would be expected in this region.

In order to apply this theory to a particular obstacle, such as the sphere in Hide & Ibbetson's experiments, we must estimate first what range of values of the radial wave-number κ will be generated locally by the obstacle. There is no need to estimate the z-component of wave-number (which actually might be more difficult) because, in terms of the x- and y-components, the z-component of wave-number of all wave energy found at large distances from the obstacle is constrained to take the form shown in (A 1). Thus, only the distribution of κ and ϕ need be estimated. Of these, κ is the more important, since it specifies through the angle (A 3) the axis of the narrow cones whereon the waves lie; by contrast, ϕ specifies merely their position *on* those cones.

Now, we know that the motion generated locally by the sphere for small Rossby number consists of a 'Taylor column', whose motion through the rest of the fluid sets up locally an approximately two-dimensional flow. The z components of wave-number of that local disturbance would, as we have said, be hard to estimate, because they are associated with the *departures* from two-dimensionality. By contrast, the x- and y-components $(\kappa\cos\phi, \kappa\sin\phi)$ can be estimated solely from a knowledge of the two-dimensional flow field to which the motion near the Taylor column approximates.

For example, if that were the irrotational motion produced by the Taylor column moving through the fluid like a solid cylinder, the x- and y-components of velocity would be

$$u = U, \quad v = 0, \quad (r \leqslant a)$$

$$u = U(a^2/r^2)\cos 2\theta, \quad v = U(a^2/r^2)\sin 2\theta, \quad (r \geqslant a), \tag{A 4}$$

where $x = r\cos\theta$, $y = r\sin\theta$ and a is the radius of the sphere. In this case the velocity spectrum for the two-dimensional flow, generated locally by the motion

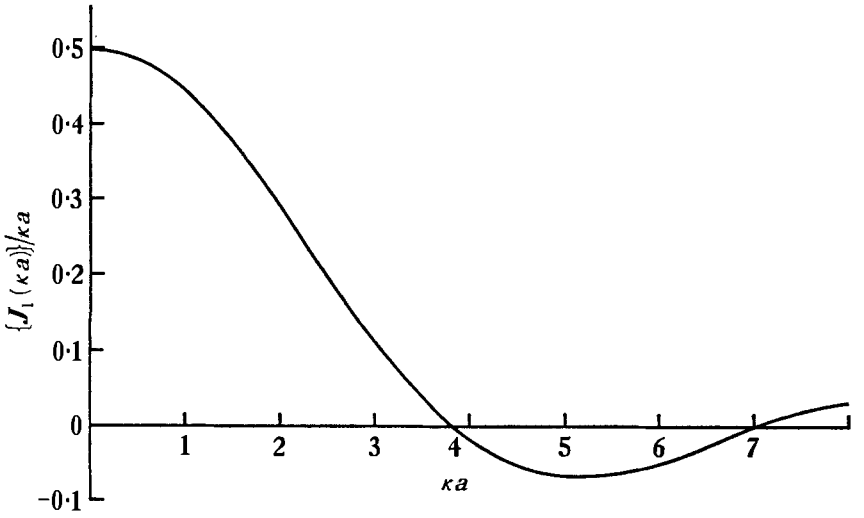

FIGURE 7

of the Taylor column, and assumed irrotational, is shown in graphical form in figure 7, which plots the variation with κ in the component of either u or v with wave-number $(\kappa\cos\phi,\ \kappa\sin\phi)$. The spectrum amplitude exceeds 13 % of its maximum value only for

$$0 \leqslant \kappa \leqslant 3{\cdot}3/a, \tag{A 5}$$

so that $3{\cdot}3/a$ might be taken as the effective upper end of the range of radial wave-numbers. The 'centroid' of the spectrum is at

$$\bar{\kappa} = \frac{\int_0^\infty \kappa[2J_1(\kappa a)/\kappa a]\,d\kappa}{\int_0^\infty [2J_1(\kappa a)/\kappa a]\,d\kappa} = \frac{1}{a}. \tag{A 6}$$

Actually, the local flow in and around the Taylor column is by no means exactly as in (A 4). Within the column some deviation from the uniform velocity $(U, 0)$ occurs, and outside it there is a still greater deviation from irrotationality. However, the general picture of the variation of velocity spectrum with κ, given by figure 7, is probably still valid for this real flow. Substantial amplitudes for values of κ exceeding about $3/a$ are unlikely, and the centroid of the spectrum is probably near $\kappa = a^{-1}$.

In support of this view is the fact that both the flow assumed (not too inaccurately) in (A 4) for $r \leqslant a$, and that assumed (somewhat less accurately) for $r \geqslant a$, *separately* have Fourier components varying with κ as in figure 7. Also streamline patterns derived experimentally give no indication of radial wave-numbers differing greatly from those associated with irrotational flow. Note that the flow (A 4) already embodies a concentrated vortex sheet at $r = a$; and that the high-wave-number end of the spectrum ought not to be increased by this vorticity being 'smudged out' into a boundary layer.

The process whereby velocity disturbances with a spectrum something like figure 7 generate waves far from the obstacle is without doubt complex, and to some extent non-linear. Accordingly, the x- and y-components ($\kappa \cos\phi$, $\kappa \sin\phi$) of wave-number of these waves may take values including not only those which are in the spectrum near the source, but also, for example, sums and differences of them. This is unlikely, however, to alter the conclusion that amplitudes will be biggest for a range of radial components of wave-number κ centred as in (A 6) on about $1/a$, where a is the radius of the sphere.

If this is so, then the centre of the disturbance associated with these waves will trail, according to (A 3), at an angle about

$$K(U/2\Omega a), \tag{A 7}$$

where $K = \frac{3}{2}$. This conclusion is well borne out by experiments described in the paper, which obtained $K = 1{\cdot}54 \pm 0{\cdot}04$ (see equations (1.3*b*) and (4.3)).

The method of observation used is, to be sure, sensitive to the z component of fluid displacement, whereas the argument picking out the radial wave-numbers that are likely to be generated started from a Fourier analysis of the x- and y-components of velocity (A 4). It might be supposed that this argument would only pick out the centre of the disturbances of x- and y-velocity at large distances. However, the z-component of fluid displacement must be directly in phase with the x- and y-components of velocity, since fluid particles in any inertial wave move in circular paths on the surfaces of constant phase, and we saw that the motion far from the obstacle is made up of inertial waves with those surfaces all making small angles with the z axis.

Again, it might be thought that the argument is wrong in using the *two-dimensional* Fourier components, proportional to $J_1(\kappa a)/\kappa a$, as an indication of wave amplitude distribution at a large distance. The distribution of wave energy might be supposed to be distorted by an additional factor κ because the area of the two-dimensional wave-number plane with values of κ lying in a given interval $(\kappa, \kappa + \delta\kappa)$ is $2\pi\kappa\,\delta\kappa$. This idea would be wrong, however, because the wave energy for which κ lies in this interval will be spread through the region between the two cones which the directions (A 2) sweep out for radial wave-numbers κ and $\kappa + \delta\kappa$. The area between these, at a cross-section $z =$ constant, is also a multiple of $\kappa\,\delta\kappa$, so that the κ factor cancels out and does not appear in the energy density far from the obstacle. The amplitude distribution is, therefore, unaffected by these considerations.

Nevertheless, the experimental agreement with the predicted value $K = \frac{3}{2}$ in (A 7) is almost embarrassingly close, since the value predicted is simply that for

the centroid of the spectrum assuming only linear generation processes, and non-linear generation processes would be expected to distort that spectrum. In fact, the agreement indicates that they do not materially alter the position of the spectrum's centroid.

Thus, we may conclude provisionally that the trailing character of disturbances generated by forcing effects in rotating fluids can be predicted to reasonable approximation by the technique (Lighthill 1967) of drawing normals to the wave-number surface in those parts of it which correspond to the wave-numbers principally excited by the forcing effect.

REFERENCES

BAKER, D. J. 1966 *J. Fluid Mech.* **26**, 573.

BRETHERTON, F. P. 1967 *J. Fluid Mech.* **28**, 545.

BRETHERTON, F. P., CARRIER, G. F. & LONGUET-HIGGINS, M. S. 1966 *J. Fluid Mech.* **26**, 393.

CHARNEY, J. G. & DRAZIN, P. 1961 *J. Geophys. Res.* **66**, 83.

GRACE, S. F. 1927 *Proc. Roy. Soc.* A **113**, 46.

HIDE, R. 1961 *Nature, Lond.* **190**, 895.

HIDE, R. 1963 *Mem. Soc. Roy. Sci. Liège* V, **7**, 481.

HIDE, R. 1966 *Bull. Am. Met. Soc.* **47**, 873.

HIDE, R. 1968 *J. Fluid Mech.* (in the Press).

HIDE, R. & IBBETSON, A. 1966 *Icarus*, **5**, 279.

JACOBS, S. J. 1964 *J. Fluid Mech.* **20**, 581.

LIGHTHILL, M. J. 1966 *J. Fluid Mech.* **26**, 411.

LIGHTHILL, M. J. 1967 *J. Fluid Mech.* **27**, 725.

LONG, R. R. 1953 *J. Meteorology*, **10**, 197.

MORGAN, G. W. 1951 *Proc. Roy. Soc.* A **206**, 108.

PROUDMAN, J. 1916 *Proc. Roy. Soc.* A **92**, 408.

ROBINSON, A. R. 1960 *J Fluid Mech.* **9**, 321.

STEWARTSON, K. 1952 *Proc. Camb. Phil. Soc.* **48**, 168.

STEWARTSON, K. 1953 *Quart. J. Mech. Appl. Math.* **6**, 141.

STEWARTSON, K. 1957 *J. Fluid Mech.* **3**, 17.

STEWARTSON, K. 1958 *Quart. J. Mech. Appl. Math.* **11**, 39.

TAYLOR, G. I. 1922 *Proc. Roy. Soc.* A **102**, 114.

TAYLOR, G. I. 1923 *Proc. Roy. Soc.* A **104**, 213.

TITMAN, C. W. 1967 In *Magnetism and the Cosmos* (ed. Hindmarsh, Lowes, Roberts and Runcorn). Edinburgh: Oliver and Boyd.

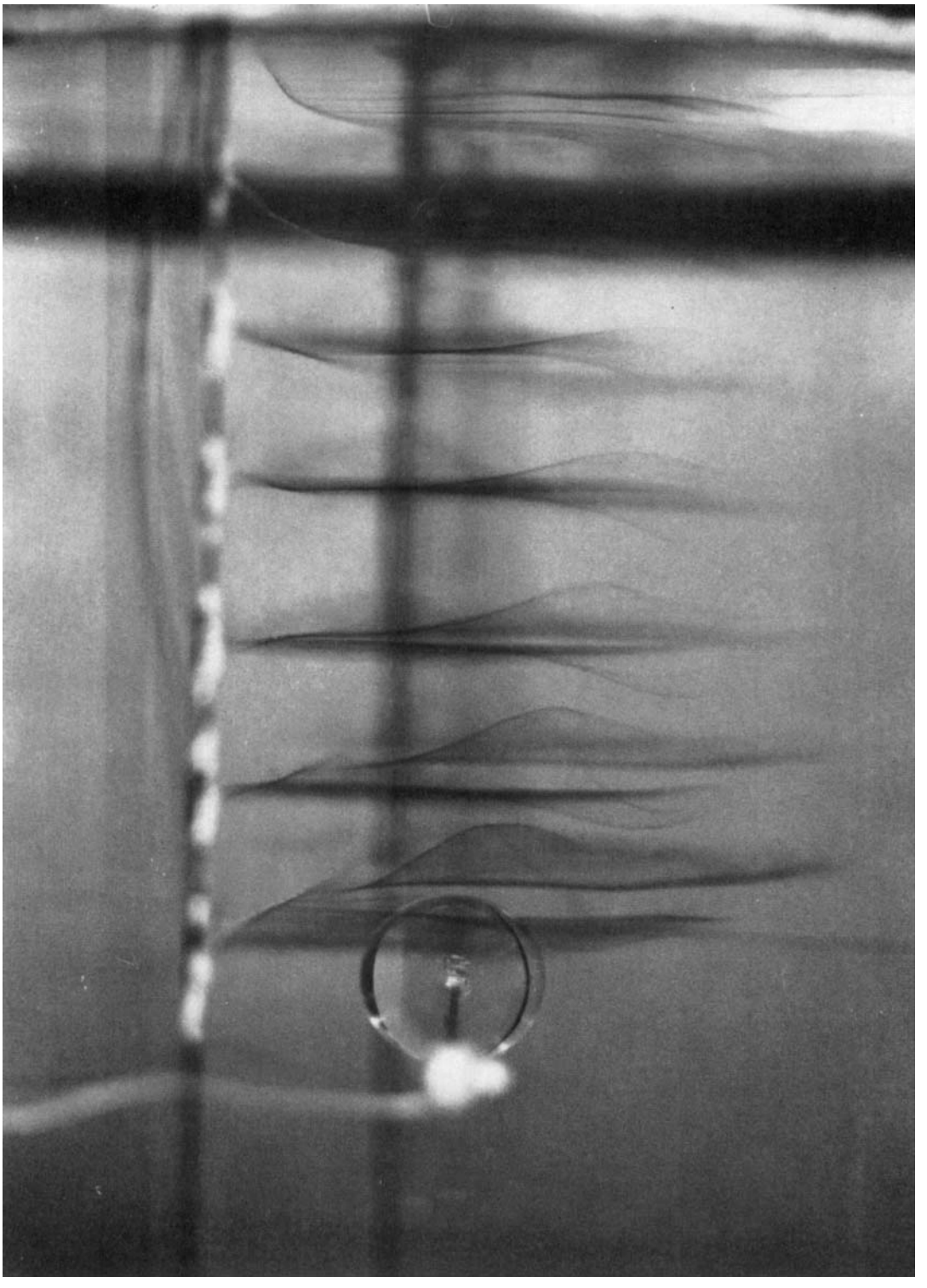

(*a*)

FIGURE 3. Illustrating the distortion of the dye sheets released by the wires upstream of a spherical obstacle looking inward along a radius through the centre of the sphere. (*a*), (*b*) and (*c*) correspond to the different Rossby numbers, $\epsilon = 0{\cdot}205$, $0{\cdot}0895$ and $0{\cdot}0336$ respectively (see table 2 for full details). ϑ increases from left to right. $\gamma = 1{\cdot}36 \times 10^{-3}$.

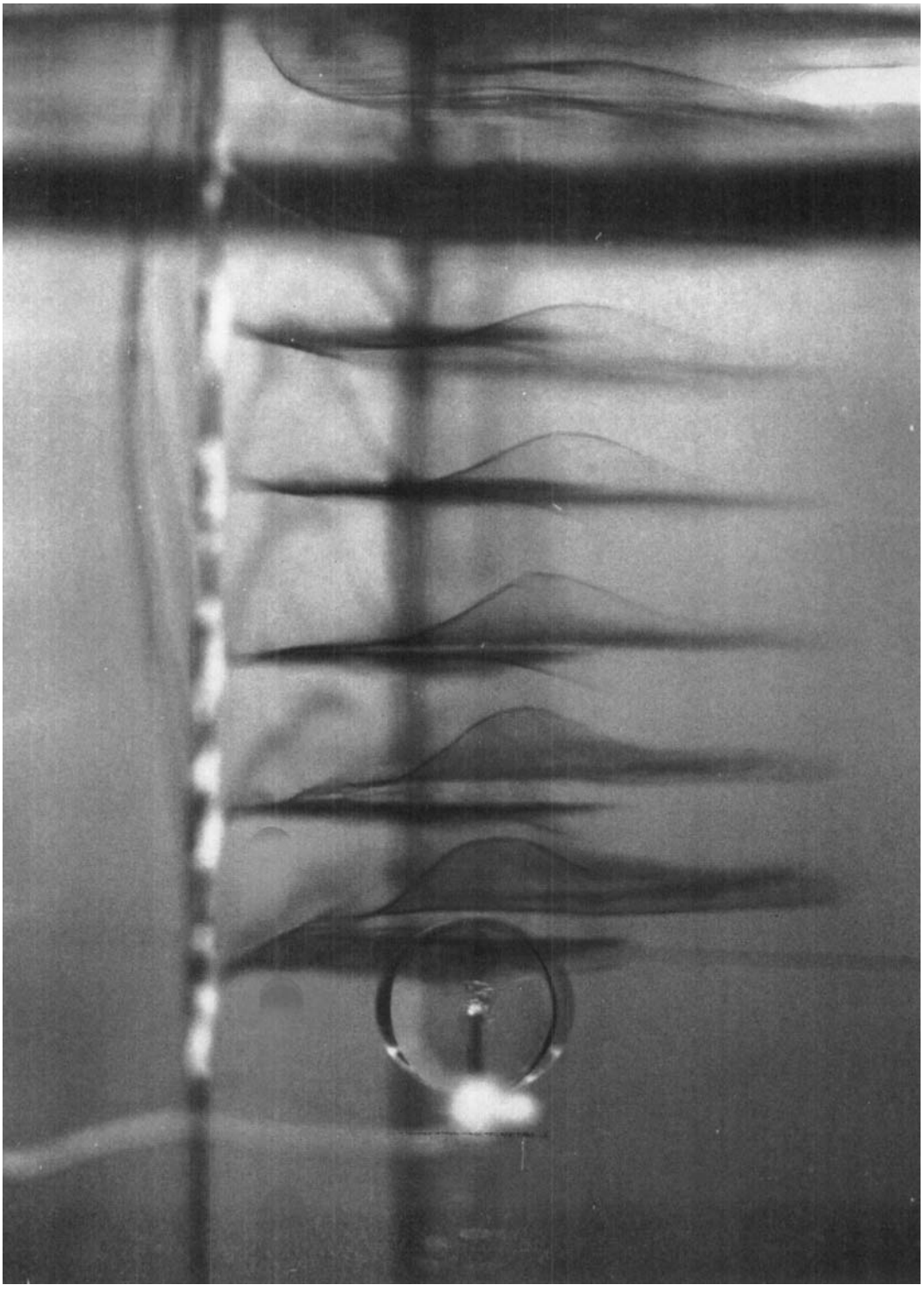

FIGURE 3(*b*). For legend see plate 1.

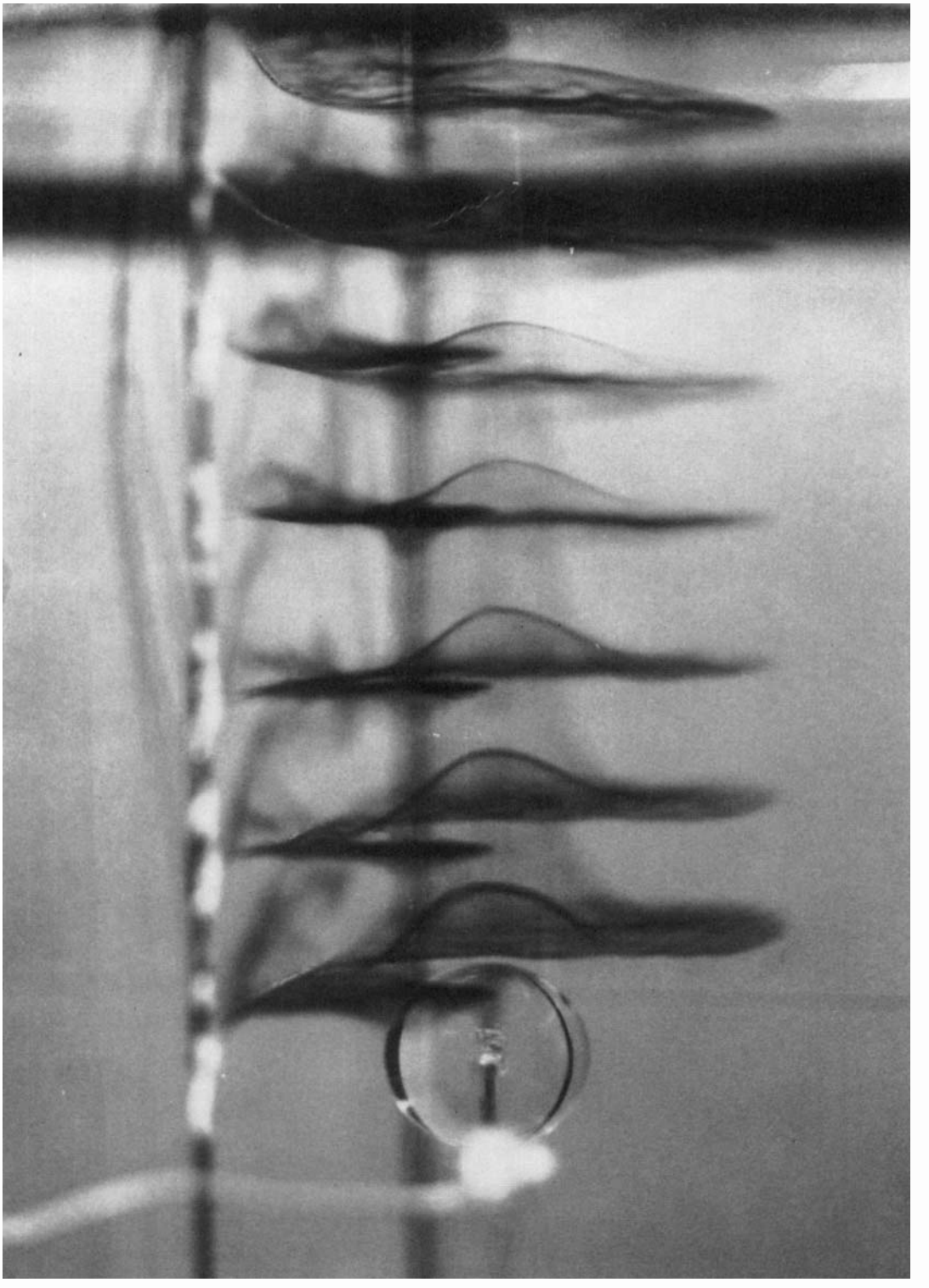

FIGURE 3(*c*). For legend see plate 1.

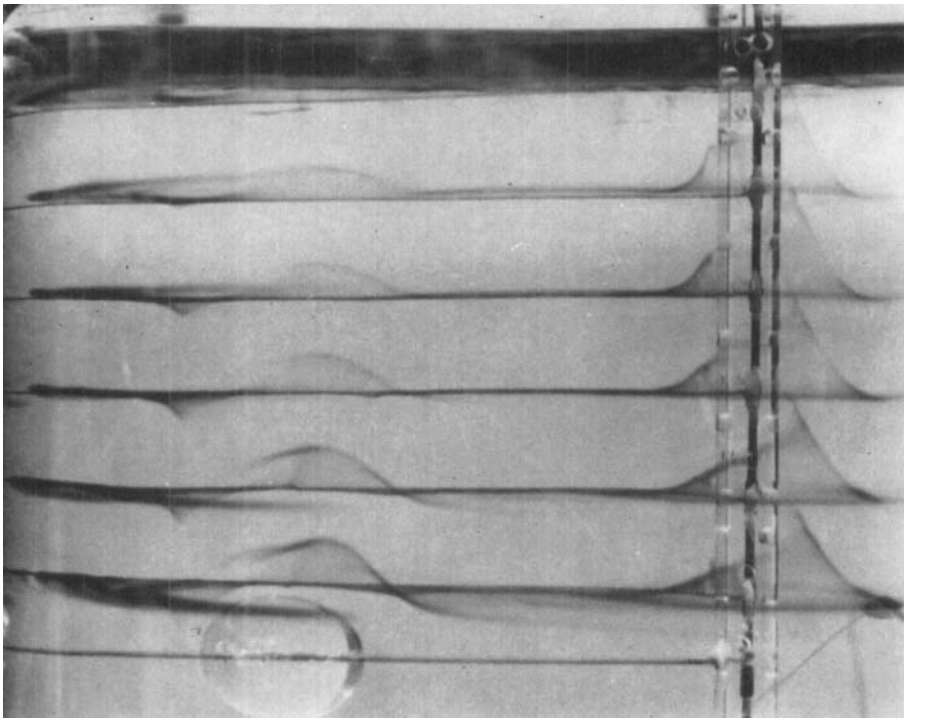

FIGURE 4(*a*)

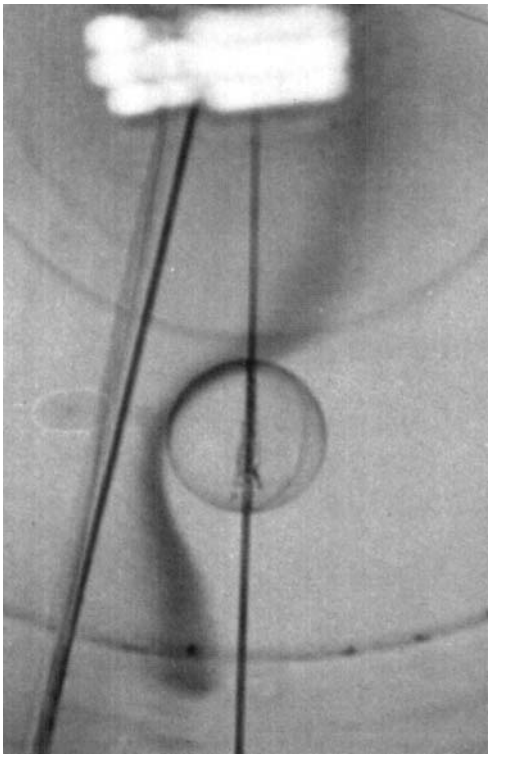

FIGURE 4(*b* i). For legend see plate 5.

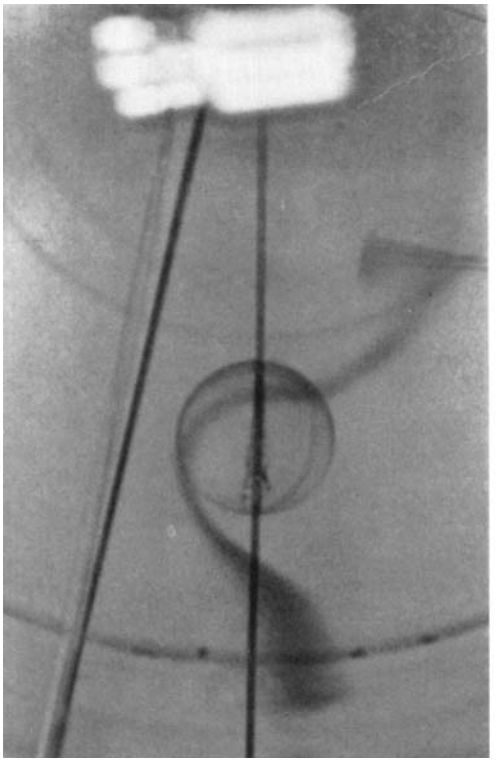

FIGURE 4 (*b* ii)

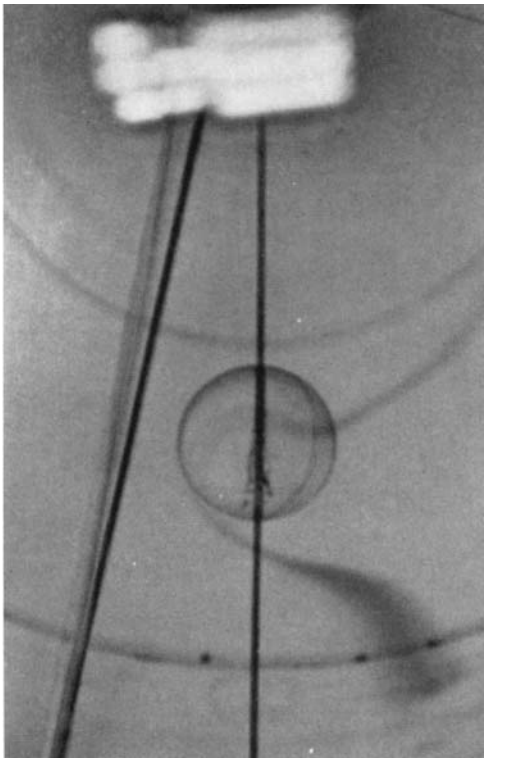

FIGURE 4 (*b* iii)

FIGURE 4 (*a*). Illustrating the distortion of the dye sheets released by the wires upstream of a spherical obstacle looking at right-angles to a radius through the centre of the sphere from downstream of the sphere. $\epsilon = 9{\cdot}01 \times 10^{-3}$, $\gamma = 1{\cdot}36 \times 10^{-3}$ (see table 2 for full details). R increases from right to left. (The distortion of the dye sheets seen at the right-hand side of the picture is due to axial motion in the vicinity of the inner wall of the annulus, in accordance with the flow illustrated in figure 1.)

(*b*) Illustrating the distortion of a line of dye released from a wire upstream of a spherical obstacle looking at right angles to the radius through the sphere in a direction parallel to the negative Z axis (rotation counterclockwise). The time intervals between consecutive pictures were approximately equal. $\epsilon = 5{\cdot}78 \times 10^{-3}$, $\gamma = 1{\cdot}32 \times 10^{-3}$ and $Z_s = 5{\cdot}0$ cm.

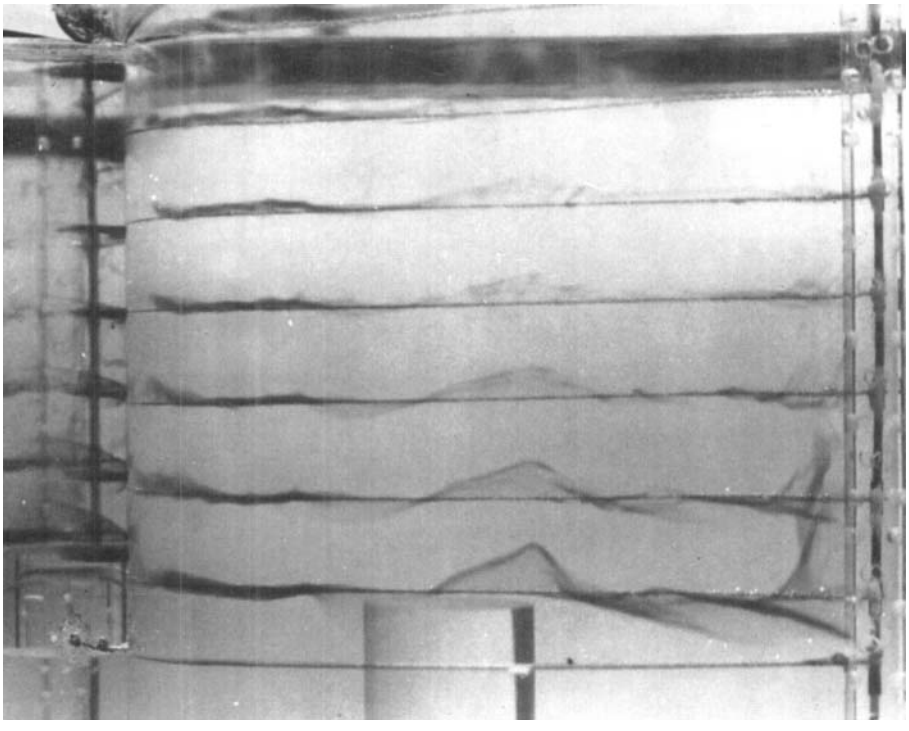

FIGURE 6 (*b*)

FIGURE 6 (*a*)

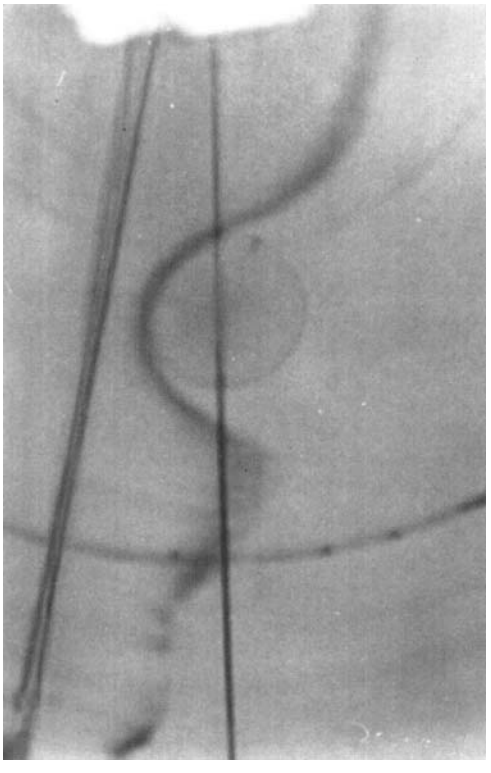

FIGURE 6 (*c* i). For legend see plate 7.

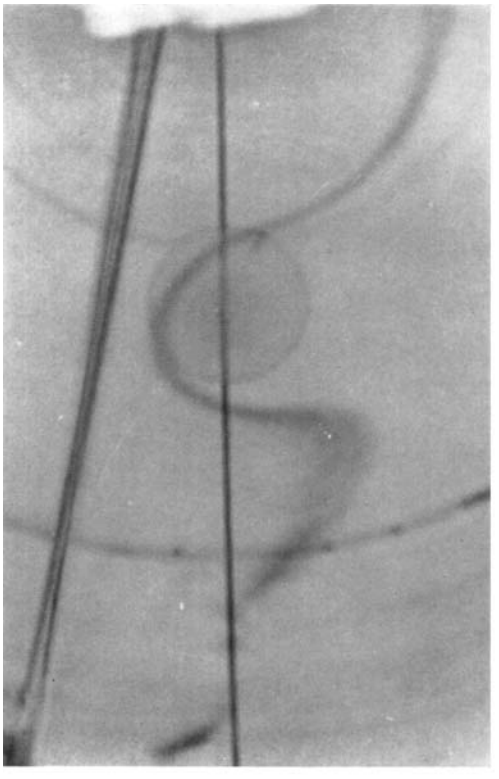

FIGURE 6(*c* ii)

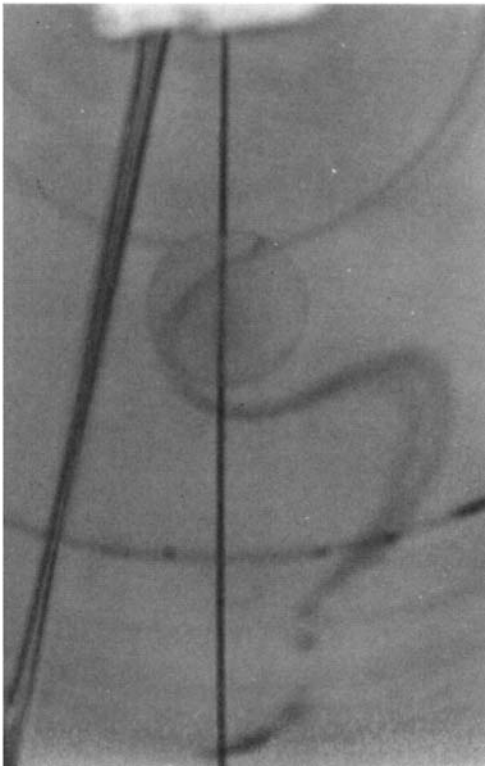

FIGURE 6(*c* iii)

FIGURE 6. Illustrating the distortion of dye sheets released by wires upstream of a cylindrical obstacle (*a*) looking inward along a radius through the centre of the cylinder, (*b*) looking at right angles to the radius through the centre of the cylinder from downstream of the cylinder, and (*c*) looking at right angles to the radius through the centre of the cylinder in a direction parallel to the negative Z axis (rotation counterclockwise); the time intervals between consecutive pictures in (*c*) were approximately the same. Experimental details: (*a*) and (*b*) $\epsilon = 9{\cdot}14 \times 10^{-3}$, $\gamma = 1{\cdot}36 \times 10^{-3}$; (*c*) $\epsilon = 1{\cdot}38 \times 10^{-2}$, $\gamma = 1{\cdot}32 \times 10^{-3}$, $Z_s = 5{\cdot}0$ cm.